AD-A165 998 REACTION INTERMEDIATES IN AROMATIC FUEL COMBUSTION(U) 1/1
CATHOLIC UNIV OF AMERICA WASHINGTON DC DEPT OF
CHEMISTRY W A SANDERS 17 JUL 85 N00014-84-C-2295
UNCLASSIFIED F/G 7/3 NL

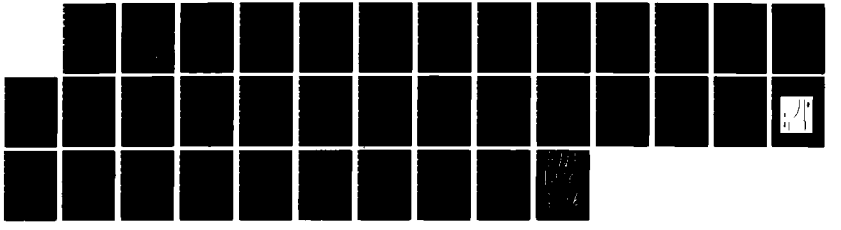

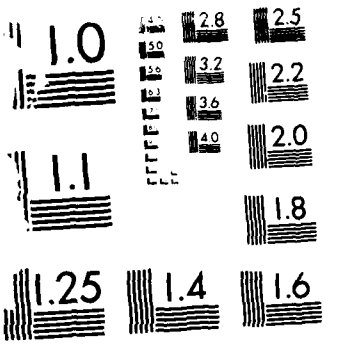

MICROCOPY RESOLUTION TEST CHART

Department of Chemistry
The Catholic University Of America
Washington D. C. 20064

Reaction Intermediates In Aromatic Fuel Combustion

Final Report

Contract No.

N00014-84-c2295

period

7-18-84 to 7-17-85

Principal Investigator: William a. Sanders

Scientific Program Officer: Dr. M. C. Lin
Naval Research Laboratory
Code 6105
4555 Overlook Ave., SW
Washington, DC 20375

ABSTRACT

The unimolecular decomposition of methylphenyl ether (anisole) was studied in incident shock waves covering the temperature range from 1000 to 1580 K and the pressure range from 0.4 to 0.9 atm. The CO formed in the reaction, monitored by resonance absorption using a stabilized cw CO laser, could be satisfactorily accounted for by a four-reaction mechanism:

$$C_6H_5OCH_3 \longrightarrow C_6H_5O + CH_3 \quad (1)$$

$$C_6H_5O \longrightarrow CO + C_5H_5 \quad (2)$$

$$CH_3 + C_6H_5O \longrightarrow o\text{- and } p\text{-}CH_3C_6H_4OH \quad (3)$$

$$CH_3 + CH_3 \longrightarrow C_2H_6 \quad (4).$$

Kinetic modeling of observed CO production profiles based on the above mechanism with 70 sets of data led to

$$k_1 \cong (1.2 \pm 0.3) \times 10^{16} \exp(-33{,}100/T) \text{ sec}^{-1},$$

$$k_2 = 10^{11.40 \pm 0.20} \exp(-22{,}100 \pm 450/T) \text{ sec}^{-1},$$

$$k_3 = (5.5 \pm 2.0) \times 10^{11} \text{ cc.mole}^{-1}.\text{sec}^{-1}.$$

The relatively low A-factor and activation energy measured for the phenoxy radical decomposition reaction supports the following mechanism involving a tight intermediate:

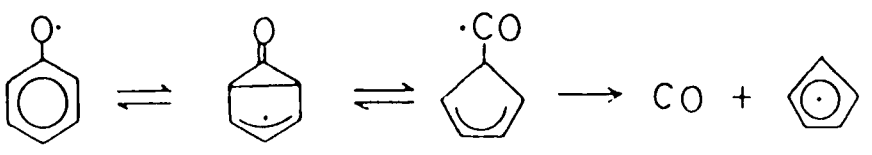

INTRODUCTION

There is increasing tendency in future fuels to have higher aromatic contents because partly of the change in fuel sources (such as coals and shale oils) and partly of the greater use of aromatic compounds as additives due to their high octane values[1].

The chemistry of the oxidation of aromatic compounds at combustion temperatures (T > 1500 K) is very complex and poorly understood[2-4]. The present study is part of a series of experiments being carried out at NRL to elucidate the oxidation mechanism of C_6H_6, the most important benchmark system for the aromatic compounds. Recent studies of C_6H_6 oxidation at high temperatures have indicated that C_6H_5OH is the most important early stage oxidation product[2-4]. In view of its known weak O-H bond[5], the C_6H_5OH generated in the early oxidation process is expected to produce C_6H_5O very readily either unimolecularly or bimolecularly via reactions with atomic and radical species[6]. Additionally, C_6H_5O may also be generated by the reaction of C_6H_6 with O atoms[7]:

$$O + C_6H_6 \longrightarrow C_6H_6O^{*\dagger} \longrightarrow C_6H_5O + H$$
$$\longrightarrow C_6H_5OH + h\nu,$$

where "$*\dagger$" stands for the vibronically excited phenol or its precursor intermediate. We have previously reported the observation of UV emission near 250 nm in C_6H_6 oxidation above 1700 K, which was attributed to the S_1 state of C_6H_5OH formed by the above reaction.[6] The understanding of the kinetics and mechanism of the C_6H_5O radical reaction at high temperatures is therefore one of the major steps toward our ultimate goal of elucidating the complex C_6H_6 oxidation chemistry.

At high temperatures, the C_6H_5O radical undergoes primarily the unimolecular decomposition reaction[9,10]

$$C_6H_5O \longrightarrow CO + C_5H_5$$
$$\Delta H^0 = 20 \text{ kcal/mole}$$

The rate constant for this reaction has not been accurately determined. Colussi et al. have estimated a value of 10 ± 5 sec^{-1} at 1000 K from their study of the allylphenyl ether decomposition reaction in a VLPP reactor[9]. In a study recently carried out in this laboratory, we have employed a cw CO laser to monitor its decomposition kinetics using methylphenyl ether (anisole) as a source of the C_6H_5O radical above 1000 K. Our preliminary results for the unimolecular decomposition of C_6H_5O evaluated on the basis of the following two-step mechanism,

$$C_6H_5OCH_3 \longrightarrow C_6H_5O + CH_3$$
$$C_6H_5O \longrightarrow CO + C_5H_5$$

have been reported elsewhere recently[6].

In this article, we analyze in detail the mechanism of anisole decomposition and the effects of secondary reactions on the kinetics of the phenoxy radical decomposition process. Additionally, we have carried out a few experiments using allylphenyl ether as the radical precursor to corroborate the measured data.

EXPERIMENTAL

The shock tube-CO laser probing apparatus is the same as that used in previous experiments carried out in this laboratory[11,12]. In this work, several highly diluted mixtures of anisole and allylphenyl ether were heated with incident shock waves. The CO formed in the decomposition reaction was detected with the $1 \longrightarrow 0$ P(10) transition of the CO laser. A detailed description of the use of stabilized cw CO lasers to measure absolute concentrations of various key combustion products, such as CO, NO and H_2O has been given recently by Hsu and Lin[13].

Anisole and allylphenyl ether, both obtained from Aldrich Chemical Co., were purified by trap-to-trap distillation prior to use. Ar (Matheson Gas Products, 99.995 % pure) was used directly to prepare various mixtures.

RESULTS

Approximate Evaluation of k_1 and k_2

Incident shock experiments were carried out in the temperature range from 1000 to 1580 K and the pressure range from 0.4 to 0.9 atm for six mixtures of anisole (0.108, 0.264, 0.519, 0.524, 0.749 and 0.758 % in Ar) and one mixture of allylphenyl ether (0.366 % in Ar).

A typical CO absorption trace is shown in Fig. 1. The absorption data were converted into CO concentration-time profiles using the calibration method described previously[11,12]. Typical relative CO production profiles are shown in Fig. 2. We have previously analyzed these CO formation rates during the early stage of decomposition according to the following two-step mechanism[6] as alluded to earlier:

$$C_6H_5OCH_3 \longrightarrow C_6H_5O + CH_3 \qquad (1)$$

$$C_6H_5O \longrightarrow CO + C_5H_5 \qquad (2)$$

On the basis of this simple scheme, the rate constants for CO formation, k_2, can be evaluated from the slopes of $\ln(1 - [CO]_t/[A]_0)$ vs. t plots at longer times according to the equations,

$$1 - \frac{[CO]_t}{[A]_0} = \frac{k_1}{k_1 - k_2}\exp(-k_2 t) - \frac{k_2}{k_1 - k_2}\exp(-k_1 t) \qquad (I)$$

and at T > 1200 K,

$$1 - \frac{[CO]_t}{[A]_0} = \frac{k_1}{k_1 - k_2}\exp(-k_2 t) \qquad (II)$$

The approximation given by eq. (II) is valid because reaction (1) is much faster than (2) above 1200 K as we have discussed before[6]. In the above equations, $[A]_0$ is the initial concentration of anisole used. Figure 3 shows different plots of eq. (I) for the same sets of data presented in Fig. 2. The slopes of the linear portions of these plots at longer reaction times should give the values of k_2 according to eq. (II), if the system is free from any secondary reactions which may effectively alter the concentration of the C_6H_5O radical. As will be discussed later, this assumption is only partially valid, particularly at lower temperatures (T < 1200 K), because of the possible occurrence of the $CH_3 + C_6H_5O$ reaction. The presence of this competing process is expected to lower the CO yields as manifested by the deficiency in the limiting values of CO mass balance shown in Fig. 2 (i.e. $[CO]_{t=\infty}/[A]_0 < 1$). Further discussion on this problem will be made below.

The values of the rate constants evaluated from the slopes of the linear portions of the plots shown in Fig. 3, denoted by k_2', are summarized in Figure 4 as well as in Table I together with other kinetic data. A least-squares analysis of these k_2' values gave rise to the apparent rate constant expression:

$$k_2' = 10^{11.90 \pm 0.20} \exp(-23{,}900 \pm 450/T) \text{ sec}^{-1}. \qquad \text{(III)}$$

This Arrhenius expression agrees very well with our preliminary results obtained from three sets of experiments ($k_2' = 10^{12.0 \pm 0.2} \exp(-24{,}000 \pm 690/T) \text{ sec}^{-1}$)[6]. It should be mentioned that the rate constants given in Fig. 4 for temperatures above 1200 K have been corrected for minor pressure dependence by means of the RRKM theory using the weak collision assumption[14].

According to eq. (I), the values of k_1 at low temperatures (T < 1200 K) can be estimated from the intercepts of the ln $(1 - [CO]_t/[A]_0)$ vs. t plots (see Fig. 3). Because of the approximate nature of the mechanism assumed and the narrow (200 K) temperature range available for k_1 evaluation, an accurate determination of the Arrhenius parameters for anisole decomposition (which is not available in the literature) is not possible. However, these approximate rate constants are useful as starting values for modeling CO formation profiles in the very early stage of anisole decomposition at low temperatures. The values of k_1 summarized in Table II for 24 sets of data have been slightly adjusted to fit exactly the observed early CO profiles. From these rate constants we can evaluate the frequency factor using the Arrhenius equation: $A_1 = k_1/\exp(-E_1/RT)$; where $E_1 \cong \Delta H_1^0 + RT = 65.8$ kcal/mole, taking $\Delta H_1^0 = 63.8$ kcal/mole[5]. The average of the 24 A_1-values summarized in Table II gave rise to $A_1 = (1.2 \pm 0.3) \times 10^{16}$ sec^{-1}. At 1000 K, the value of $k_1 = 50$ sec^{-1} estimated by $k_1 = 1.2 \times 10^{16} \exp(-65{,}800/RT)$ sec^{-1} can be compared with that for the decomposition of ethylphenyl ether in the high-pressure limit determined by Colussi et al.[9], 126 sec^{-1}.

Evaluation of k_2 and k_3 by Kinetic Modeling

The deficiency in CO mass balance mentioned before is believed to result from the CH_3 + C_6H_5O reaction which can competitively remove the phenoxy radical. This reaction has been previously shown to form o- and p-cresols via methylcyclohexadienones by Mulcahy and Williams[15,16]:

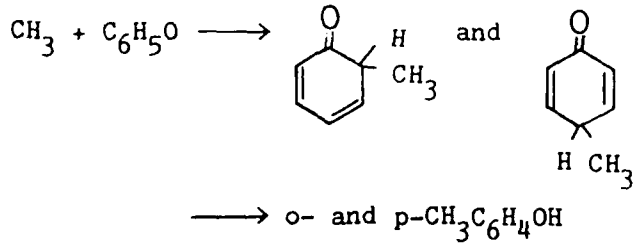

The occurrence of this reaction can account for the formation of cresols in the pyrolysis of anisole at lower temperatures[17,18]. The above combination mechanism is quite reasonable in view of the possible existence of the following resonance structures [15,16]:

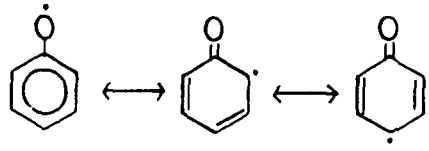

The cresols thus formed are thermochemically much more stable than anisole and the phenoxy radical. Accordingly, their formation depletes the yield of CO, leading to the apparent loss of CO and thus the deviation from linearity in the ln (1 - $[CO]_t/[A]_0$) vs. t plots as shown in Fig. 3.

To correct the effects of this side reaction, we have attempted to computer-model the production of CO using the following mechanism:

$$C_6H_5OCH_3 \longrightarrow C_6H_5O + CH_3 \qquad (1)$$

$$C_6H_5O \longrightarrow CO + C_5H_5 \qquad (2)$$

$$CH_3 + C_6H_5O \longrightarrow o\text{-} \;\&\; p\text{-}CH_3C_6H_4OH \qquad (3)$$

$$CH_3 + CH_3 \longrightarrow C_2H_6 \qquad (4)$$

The modeling could be readily done by varying k_3 (which is not known) to fit the observed $[CO]_t/[A]_0$ values at long reaction times and simultaneously fine-tuning the values of k_2, which were initially set as k_2', to account for the rising portions of the CO formation profiles. The values of k_1 obtained from the preceding section, $k_1 = 1.2 \times 10^{16} \exp(-65{,}800/RT)\ sec^{-1}$, and k_4 by Glänzer et al.[19] with appropriate pressure dependence corrections were used without adjustment. The simple kinetic modeling quickly led to convergence in the values of k_2 and k_3 because the corrections for the observed deviations in CO yields from those predicted by the two-step scheme presented in the preceding section are usually not very large at low temperatures and were found to be quite small above 1200 K, at which reaction (2) becomes very fast. Some of the modeled data are shown in Figures 5-7, together with the results of sensitivity tests for k_2 and k_3.

The values of k_2 and k_3 derived from kinetic modeling are summarized in Table I. The Arrhenius plot for k_2 is presented in Fig. 8. The least-squares analysis of k_2, after minor corrections for pressure effect at high temperatures, led to the following expression,

$$k_2 = 10^{11.40 \pm 0.20} \exp(-22{,}100 \pm 450/T)\ sec^{-1} \qquad (IV)$$

The slightly lower values for the A-factor and E_a, in comparison with those given in eq. (III), result essentially from the slightly increased value of k_2 below 1200 K where the effect of reaction (3) is larger.

The values of k_3 fall in the range of (1-10) x 10^{11} cc.mole^{-1}.sec^{-1} with the averaged value of (5.5 ± 2.0) x 10^{11} cc.mole^{-1}.sec^{-1}, which seems reasonable for such a combination reaction. Further analysis of this mechanistically very interesting reaction is still underway.

Aside from reactions (3) and (4) included in the above mechanism, we have also tested the possible influence of the following reactions on CO formation, including the reverse of reaction (2):

$$CO + C_5H_5 \longrightarrow C_6H_5O \qquad (-2)$$

$$CH_3 + C_5H_5 \rightleftharpoons C_6H_8 \qquad (5), (-5)$$

$$CH_3 + CO + M \rightleftharpoons CH_3CO + M \qquad (6), (-6)$$

$$CH_3 + CH_3CO \longrightarrow CH_3COCH_3 \qquad (7)$$

$$C_6H_5O + CH_3CO \longrightarrow CH_3COOC_6H_5 \qquad (8)$$

These processes were, however, found to have negligible effects on the observed CO formation profiles over the whole range of conditions employed. The rate constants for reactions (-2) and (-5) were estimated by the equilibrium constants calculated from the known thermochemistry of C_5H_5 and group additivity rules[20]. They are summarized in Table III together with other rate constants used in the modeling calculations.

DISCUSSION

The observed CO production profiles from six different, highly diluted mixtures of anisole (0.1 - 0.75 % in Ar) in the temperature range of 1000 - 1580 K could be quantitatively accounted for with the mechanism consisting of reactions (1)-(4). Reaction (2) is believed to be the sole source of CO. It is responsible for nearly

all of the phenoxy radical disappearance rates above 1200 K. The observed limiting CO yields, $[CO]_{t=\infty}$, however, were always found to be less than the starting concentrations of anisole, $[A]_0$. This deficiency in CO mass balance was attributed to the occurrence of reaction (3), which has previously been shown to produce o- and p-cresols, $CH_3C_6H_4OH$. Since cresols are thermochemically much more stable than both anisole and the phenoxy radical, their production at lower temperatures (at which the C_6H_5O decomposition reaction is comparably slow) effectively reduces the yield of CO as was experimentally observed.

Kinetic modeling of CO production profiles based on the above relatively simple scheme led to:

$$k_2 = 10^{11.40 \pm 0.20} \exp(-22{,}100 \pm 450/T) \text{ sec}^{-1}$$

$$k_3 = (5.5 \pm 2.0) \times 10^{11} \text{ cc.mole}^{-1}.\text{sec}^{-1}$$

covering the temperature range of 1000 - 1580 K. For k_2 the slight pressure effect, which is more pronounced at the high temperature end, has been corrected by means of the RRKM theory based on the weak collision model[14].

To corroborate the measured C_6H_5O decomposition rates, particularly for the lower temperature end of this study ($T \leq 1100$ K) which is subject to a slightly larger uncertainty because of the $CH_3 + C_6H_5O$ reaction, we have employed allylphenyl ether as the source of C_6H_5O radicals. The much lower activation energy for C_6H_5O production from this source[9] and the lower reactivity of the allyl radical in comparison with CH_3 allow us to extend the temperature down to 900 K. The results obtained from the decomposition of the 0.366 % allylphenyl ether/Ar mixture in incident shocks are included in Figure 8 for comparison. These data are seen to be

in full agreement with those obtained from anisole decomposition. It should be mentioned that the $[CO]_{t=\infty}/[A]_0$ ratios measured at higher temperatures were found to be scattered around unity, suggesting that the recombination of C_6H_5O with C_3H_5 is comparatively unimportant. Further study of this reaction system seems to be worthwhile, especially using a heated shock tube (to alleviate the low vapor-pressure problem associated with the system).

The values of k_3 summarized in Table II were within the range of $(1 - 10) \times 10^{11}$ $cc.mole^{-1}.sec^{-1}$. The activation energy for the recombination process, $CH_3 + C_6H_5O$, could not be reliably determined due to the scatter of the data. The values of k_3 appear to be reasonable for this type of process involving the rather unreactive C_6H_5O radical. Currently, we are in the process of analyzing the mechanism of this interesting reaction (which involves 1,3-sigmatropic hydrogen transfer) using the formulation put forward by us previously on the basis of the RRKM theory to account for the kinetics of high temperature processes that occur via long-lived intermediates[12,21]. The results of this analysis will be discussed in a separate report.

The relatively small frequency factor (2.5×10^{11} sec^{-1}) and activation energy (44.0 ± 0.9 kcal/mole) for the unimolecular decomposition of the C_6H_5O radical determined here is most interesting. Benson and coworkers[9] have previously proposed two possible mechanisms to account for the formation of CO and C_5H_5:

Mechanism A:

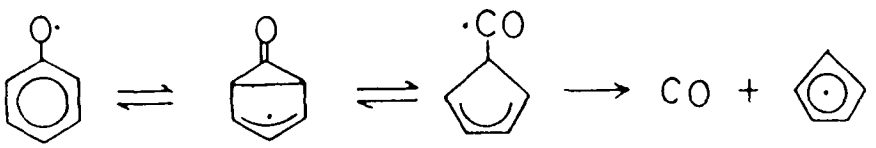

Mechanism B:

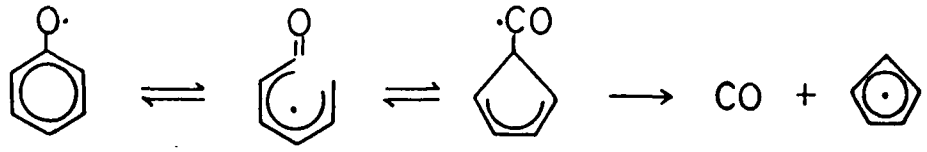

They favored mechanism A on the basis of the estimated k_2 at 1000 K and on other thermochemical grounds. The apparent low A-factor and activation energy measured in this study seem to render a very strong support for this tight-complex mechanism. The alternate mechanism (B) would perhaps require a much larger activation energy, together with a "normal" A-factor of $\geq 10^{13.5}$ sec^{-1}, for the ring-opening process.

CONCLUSION

The kinetics of the unimolecular reaction of the C_6H_5O radical has been investigated in a shock tube using a stabilized CO laser to monitor the production of CO. Both anisole and allylphenyl ether were employed as phenoxy radical sources. The kinetic modeling of observed CO production profiles obtained from about 70 sets of experiments covering 1000 - 1580 K gave rise to the rate constants:

$$k_2 = 10^{11.40 \pm 0.20} \exp(-22{,}100 \pm 450/T)\ sec^{-1}$$

and

$$k_3 = (5.5 \pm 2.0) \times 10^{11}\ cc.mole^{-1}.sec^{-1}$$

for the unimolecular decomposition of C_6H_5O and the reaction of CH_3 with C_6H_5O, respectively. The relatively low values of the A-factor and activation energy for the C_6H_5O decomposition reaction favor the mechanism that involves a bicyclic radical intermediate. Additionally, the modeling of CO yields in the very early stage of anisole decomposition at temperatures below 1200 K gave rise to the following approximate rate constant for the unimolecular decomposition process:

$$k_1 \cong (1.2 \pm 0.3) \times 10^{16} \exp(-33{,}100/T) \text{ sec}^{-1}.$$

The rate constant determined hereon for this important process is expected to be useful for the interpretation of the complex C_6H_6 combustion chemistry.

REFERENCES

(1) Longwell, J. P., in "Alternate Hydrocarbon Fuels: Combustion and Chemical Kinetics", Eds. C. T. Bowman, and J. Birkeland, p3, AIAA, 1978.

(2) Bittner, J. D., and Howard, J. B., 18th Symp. (Int.) on Combust., p1105, The Combustion Institute, 1981.

(3) Venkat, C., Brezinsky, K., and Glassman, I., 19th Symp. (Int.) on Combust., p143, The Combustion Institute, 1982.

(4) Bittner, J. D., Howard, J. B., and Palmer, H. B., NATO Conf. Ser. VI, Material Sci., vol. 7, p95, Plenum Press, 1983.

(5) McMillen, D. F., and Golden, D. M., Ann. Rev. Phys. Chem., 1982, 33, 493.

(6) Lin, C.-Y., and Lin, M. C., Int. J. Chem. Kinet., in press.

(7) Sibener, S. J., Buss, R. J., Casavecchia, P., Hirooka, T., and Lee, Y. T., J. Chem. Phys., 1980, 72, 4341.

(8) Hsu, D. S. Y., Lin, C.-Y., and Lin, M. C., 20th Symp. (Int.) on Combust., pxxx, The Combustion Institute, 1985, in press.

(9) Colussi, A. J., Zabel, F., and Benson, S. W., Int. J. Chem. Kinet., 1977, 9, 161.

(10) Harrison, A. G., Honnen, L. R., Dauben, H. J., and Lossing, F. P., J. Am. Chem. Soc., 1960, 82, 5593.

(11) Hsu, D. S. Y., Shaub, W. M., Blackburn, M., and Lin, M. C., 19th Symp. (Int.) on Combust., p89, The Combustion Institute, 1982.

(12) Hsu, D. S. Y., Shaub, W. M., Creamer, T., Gutman, D., and Lin, M. C., Ber. Bunsenges. Phys. Chem., 1983, 87, 909.

(13) Hsu, D. S. Y., and Lin, M. C., in "Applications of Laser Chemistry and Diagnostics", Ed. A. B. Harvey, vol. 482, p79, SPIE, Bellingham, WA, 1984.

(14) Troe, J., J. Phys. Chem., 1979, 83, 114.

(15) Mulcahy, M. F. R., and Williams, D. J., Nature, 1963, 199, 761.

(16) Mulcahy, M. F. R., and Williams, D. J., Aust. J. Chem., ~~1964, 17, 1329.~~ 1965, 18, 20

(17) Kislitsyn, A. N., Savinykh, V. I., and Latysheva, V. A., Zh. Prikl. Khim., 1972, 45, 384.

(18) Bredenberg, J. B., and Ceylan, R., Feul, 1983, 62, 342.

(19) Glänzer, K., Quack, M., and Troe, J., Chem. Phys. Lett., 1976, 39, 304.

(20) Benson, S. W., "Thermochemical Kinetics", J. Wiely and Sons, N. Y., 1976.

(21) Berman, M. R., and Lin, M. C., J. Phys. Chem., 1983, 87, 3933.

TABLES

Table I. Experimental data and evaluated rate constants for reactions (2) and (3).

Mixture*	P (atm)	T (K)	k_2' (sec^{-1})	k_2 (sec^{-1})	k_3 ($cc.mole^{-1}.sec^{-1}$)
A	0.659	1186	1.2×10^3	1.5×10^3	5.0×10^{11}
A	0.636	1166	1.5×10^3	2.1×10^3	3.0×10^{11}
A	0.609	1159	5.1×10^3	6.5×10^3	7.0×10^{11}
A	0.582	1334	1.6×10^4	1.9×10^4	7.0×10^{11}
A	0.823	1192	1.7×10^3	2.5×10^3	8.0×10^{11}
A	0.786	1257	5.5×10^3	6.0×10^3	7.0×10^{11}
A	0.782	1149	1.4×10^3	2.3×10^3	1.0×10^{12}
A	0.799	1265	5.5×10^3	7.5×10^3	4.0×10^{11}
A	0.737	1318	1.1×10^4	1.4×10^4	8.0×10^{11}
A	0.784	1119	8.9×10^2	1.3×10^3	4.0×10^{11}
A	0.792	1216	3.4×10^3	4.5×10^3	5.0×10^{11}
A	0.567	1301	8.9×10^3	1.1×10^4	8.0×10^{11}
A	0.755	1400	3.1×10^4	3.5×10^4	7.0×10^{11}
A	0.645	1180	1.8×10^3	2.7×10^3	6.0×10^{11}
A	0.804	1177	1.6×10^3	2.3×10^3	9.0×10^{11}
A	0.809	1155	1.4×10^3	2.0×10^3	9.0×10^{11}
A	0.839	1144	9.1×10^2	1.4×10^3	9.0×10^{11}
B	0.658	1173	8.8×10^2	1.3×10^3	3.0×10^{11}
B	0.681	1085	3.9×10^2	4.5×10^2	

Table I. (Cont'd)

B	0.749	1083	5.5×10^{2}	5.5×10^{2}	2.0×10^{11}
B	0.619	1233	3.1×10^{3}	5.0×10^{3}	6.0×10^{11}
B	0.584	1345	1.8×10^{4}	2.3×10^{4}	6.0×10^{11}
B	0.587	1299	1.3×10^{4}	1.5×10^{4}	6.0×10^{11}
B	0.559	1391	3.1×10^{4}	3.3×10^{4}	8.0×10^{11}
B	0.491	1470	7.0×10^{4}	1.0×10^{5}	8.0×10^{11}
B	0.684	1131	6.0×10^{2}	8.0×10^{2}	1.0×10^{11}
B	0.493	1586	1.2×10^{5}	1.2×10^{5}	4.0×10^{11}
B	0.514	1361	3.3×10^{4}	3.0×10^{4}	2.0×10^{11}
B	0.639	1190	2.0×10^{3}	3.0×10^{3}	8.0×10^{11}
B	0.658	1129	8.8×10^{2}	1.0×10^{3}	
C	0.631	1186	1.4×10^{3}	2.4×10^{3}	7.0×10^{11}
C	0.599	1347	1.0×10^{4}	1.2×10^{4}	9.0×10^{11}
C	0.520	1430	4.0×10^{4}	4.0×10^{4}	6.0×10^{11}
C	0.655	1146	3.4×10^{2}	1.2×10^{3}	8.0×10^{11}
C	0.643	1201	1.1×10^{3}	1.6×10^{3}	5.5×10^{11}
C	0.612	1234	2.4×10^{3}	3.0×10^{3}	3.0×10^{11}
C	0.595	1293	1.1×10^{4}	1.1×10^{4}	3.0×10^{11}
C	0.585	1343	1.6×10^{4}	1.7×10^{4}	5.0×10^{11}
C	0.651	1182	5.9×10^{2}	1.3×10^{3}	4.0×10^{11}
C	0.499	1428	4.8×10^{4}	5.0×10^{4}	4.0×10^{11}
D	0.631	1153	6.8×10^{2}	1.4×10^{3}	5.0×10^{11}
D	0.819	1111	4.5×10^{2}	1.0×10^{3}	3.5×10^{11}
D	0.867	1114	3.6×10^{2}	4.0×10^{2}	1.0×10^{11}

Table I. (Cont'd)

D	0.927	1096	1.6×10^{2}	2.5×10^{2}	1.0×10^{11}
D	0.698	1143	4.7×10^{2}	6.0×10^{2}	4.0×10^{11}
D	0.727	1066	1.4×10^{2}	3.0×10^{2}	
D	0.771	1066	8.3×10^{1}	2.0×10^{2}	
D	0.672	1114	4.0×10^{2}	3.5×10^{2}	
D	0.524	1431	4.9×10^{4}	6.5×10^{4}	6.0×10^{11}
D	0.535	1321	1.2×10^{4}	1.7×10^{4}	6.0×10^{11}
D	0.500	1423	4.1×10^{4}	5.5×10^{4}	8.0×10^{11}
D	0.472	1431	6.1×10^{4}	6.5×10^{4}	8.0×10^{11}
D	0.656	1157	5.1×10^{2}	7.5×10^{2}	4.0×10^{11}
E	0.697	1062	6.0×10^{1}	1.7×10^{2}	4.0×10^{11}
E	0.662	1124	2.4×10^{2}	5.0×10^{2}	4.0×10^{11}
E	0.625	1138	4.0×10^{2}	8.0×10^{2}	5.0×10^{11}
E	0.566	1151	8.4×10^{2}	1.6×10^{3}	6.0×10^{11}
E	0.595	1268	3.0×10^{3}	4.5×10^{3}	7.0×10^{11}
E	0.693	1017	3.5×10^{1}	1.2×10^{2}	2.0×10^{11}
E	0.552	1311	5.5×10^{3}	7.5×10^{3}	6.5×10^{11}
E	0.508	1403	2.2×10^{4}	3.0×10^{4}	7.0×10^{11}
F	0.653	1162	5.3×10^{2}	1.0×10^{3}	7.0×10^{11}
F	0.726	1038	6.9×10^{1}	1.5×10^{2}	
F	0.745	1015	2.8×10^{1}	1.5×10^{2}	4.0×10^{11}
F	0.724	1072	1.0×10^{2}	2.3×10^{2}	4.0×10^{11}
F	0.692	1131	3.3×10^{2}	5.0×10^{2}	2.0×10^{11}
F	0.586	1217	2.1×10^{3}	3.3×10^{3}	9.0×10^{11}

Table I. (Cont'd)

F	0.568	1336	8.4×10^{3}	1.0×10^{4}	5.0×10^{11}
F	0.494	1361	1.7×10^{4}	2.3×10^{4}	9.0×10^{11}
F	0.475	1491	5.4×10^{4}	6.6×10^{4}	4.0×10^{11}
F	0.439	1486	6.5×10^{4}	7.5×10^{4}	6.0×10^{11}
F	0.704	1038	6.1×10^{1}	2.3×10^{2}	1.0×10^{11}
F	0.498	1427	3.6×10^{4}	3.6×10^{4}	3.0×10^{11}

* Mixture A: 0.108 % anisole in Ar

Mixture B: 0.264 % anisole in Ar

Mixture C: 0.519 % anisole in Ar

Mixture D: 0.524 % anisole in Ar

Mixture E: 0.749 % anisole in Ar

Mixture F: 0.758 % anisole in Ar

Table II. Estimated first order rate constants for anisole decomposition.

Mixture*	P (atm)	T (K)	k_1 (sec^{-1})	A_1 (sec^{-1})+
B	0.684	1131	2.9×10^3	1.5×10^{16}
B	0.749	1083	7.9×10^2	1.5×10^{16}
B	0.681	1085	8.3×10^2	1.5×10^{16}
C	0.655	1146	4.2×10^3	1.5×10^{16}
C	0.651	1182	1.0×10^4	1.5×10^{16}
C	0.631	1186	1.1×10^4	1.5×10^{16}
D	0.672	1114	1.2×10^3	9.8×10^{15}
D	0.727	1066	3.2×10^2	9.9×10^{15}
D	0.771	1066	3.3×10^2	1.0×10^{16}
D	0.698	1143	2.6×10^3	1.0×10^{16}
D	0.819	1111	1.1×10^3	9.8×10^{15}
D	0.867	1114	1.2×10^3	9.8×10^{15}
D	0.927	1096	7.6×10^2	1.0×10^{16}
D	0.631	1154	3.7×10^3	1.1×10^{16}
E	0.693	1017	1.4×10^2	2.0×10^{16}
E	0.697	1062	2.8×10^2	9.8×10^{15}
E	0.566	1151	4.8×10^3	1.5×10^{16}
E	0.662	1124	1.6×10^3	9.9×10^{15}
E	0.625	1138	3.0×10^3	1.3×10^{16}
F	0.745	1015	1.2×10^2	1.8×10^{16}
F	0.724	1072	3.9×10^2	1.0×10^{16}

Table II. (cont'd)

F	0.704	1038	1.4×10^2	1.0×10^{16}
F	0.726	1038	1.4×10^2	1.0×10^{16}
F	0.692	1131	1.9×10^3	9.9×10^{15}

averaged value of A_1 : $(1.2 \pm 0.3) \times 10^{16}$

---

* for mixture composition, see the footnote for Table I.

+ $A_1 = k_1/\exp(-65{,}800/RT)$.

Table III. Rate constants used in the kinetic modeling of CO production, $k = AT^n \exp(-E/RT)$ (A in cc, mole, sec units and E in kcal/mole).

Reaction	A	n	E	Remarks
1	1.2×10^{16}	0	65.8	This work, see text.
2	2.5×10^{11}	0	44.0	This work, see text.
-2	8.6×10^{8}	0	26.9	Calculated from k_2 and K_2[a].
3	$(1 - 10) \times 10^{11}$	0	0	This work, see text.
4	$(2 - 5) \times 10^{12}$	0	0	Ref. 17, depending on pressure.
5	1.0×10^{12}	0	0	Assumed.
-5	4.8×10^{14}	0	58.5	Calculated from k_5 and K_5[b].
6	1.2×10^{23}	-2.8	7.6	c
-6	1.9×10^{22}	-1.7	16.7	c
7	2.4×10^{13}	0	0	c
8	1.0×10^{12}	0	0	Assumed.

a. $K_2 = 2.9 \times 10^{2} \exp(-17{,}100/RT)$ mole.cc^{-1}.

b. $K_5 = 2.1 \times 10^{-3} \exp(58{,}500/RT)$ cc.mole^{-1}.

c. Based on a recent compilation and recommendation by W. Tsang.

FIGURES

Fig. 1. A typical CO laser absorption trace (T = 1321 K, P = 0.535 atm, using 0.524 % anisole in Ar).

Fig. 2. Typical relative CO production profiles.
Triangles: T = 1111 K, P = 0.819 atm, 0.524 % anisole in Ar.
Circles: T = 1217 K, P = 0.586 atm, 0.758 % anisole in Ar.
Reversed triangles: T = 1311 K, P = 0.552 atm, 0.749 % anisole in Ar.

Fig. 3. Ln $(1 - [CO]_t/[A]_0)$ vs. t plots for same sets of data in Fig. 2.

Fig. 4. The Arrhenius plot for k_2'.

Fig. 5. Observed and modeled CO production profiles at 1403 K for 0.749 % anisole/Ar mixture at P = 0.508 atm; circles: experimental results, solid line: modeled result using the mechanism including reactions (1-4), dashed lines: sensitivity tests for k_2 (figure a) and k_3 (figure b). The test results clearly show that the computed CO yield in the rising portion of the production profile depends much more sensitively on the value of k_2 than k_3, whereas the CO yield in the plateau region at longer reaction times varies more strongly with k_3 than k_2. These effects facilitate the convergency of k_2 and k_3 immensely.

Fig. 6. Observed and modeled CO production profiles at 1268 K for 0.749 % anisole/Ar mixture at P = 0.595 atm; symbols are the same as those in Fig. 5.

Fig. 7. Observed and modeled CO production profiles at 1143 K for 0.524 % anisole/Ar mixture at P = 0.698 atm; symbols are the same as those in Fig. 5.

Fig. 8 The Arrhenius plot for k_2. The Arrhenius expression, $k_2 = 10^{11.40 \pm 0.20} \exp(-22{,}100 \pm 450/T)\ sec^{-1}$, was obtained from the least-squares analysis of data from six different mixtures of anisole in Ar.

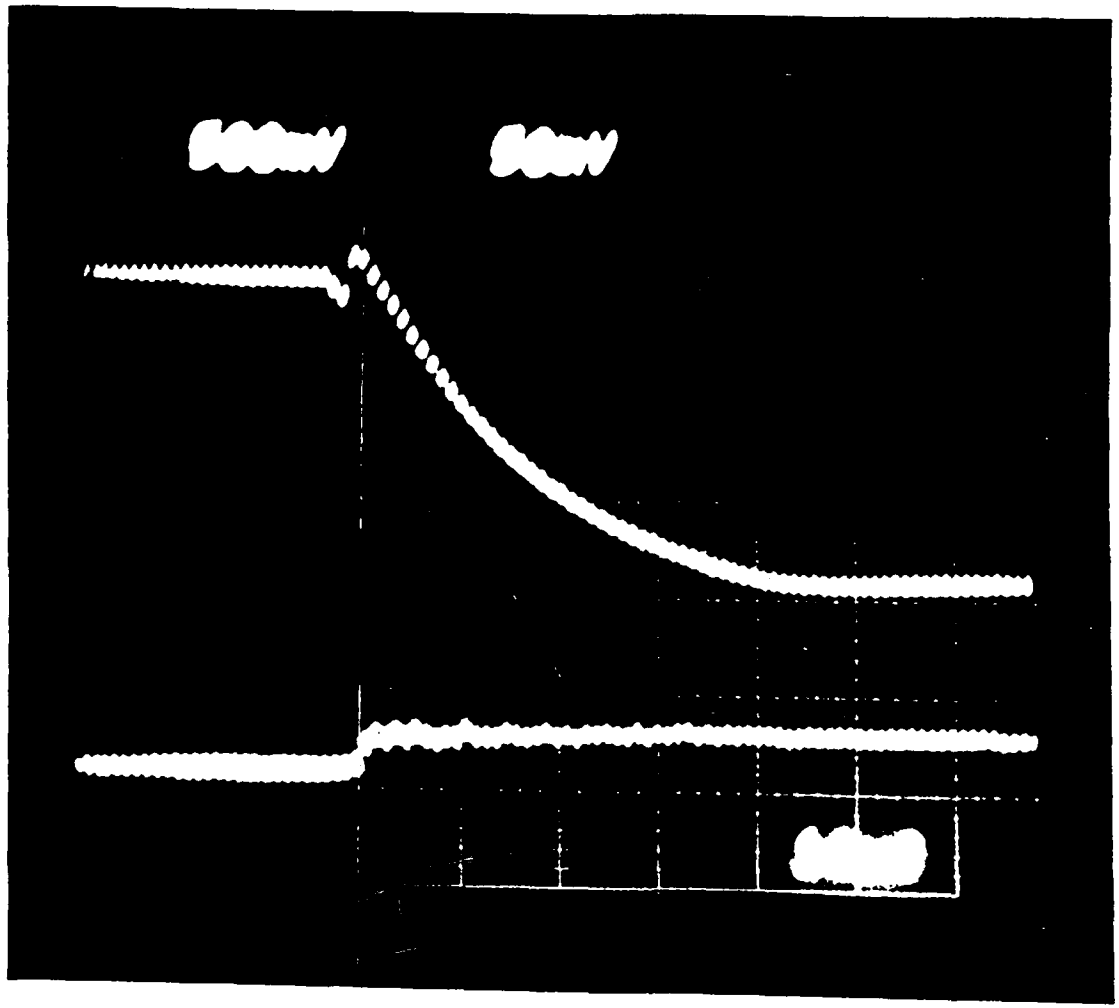

Fig. 1.

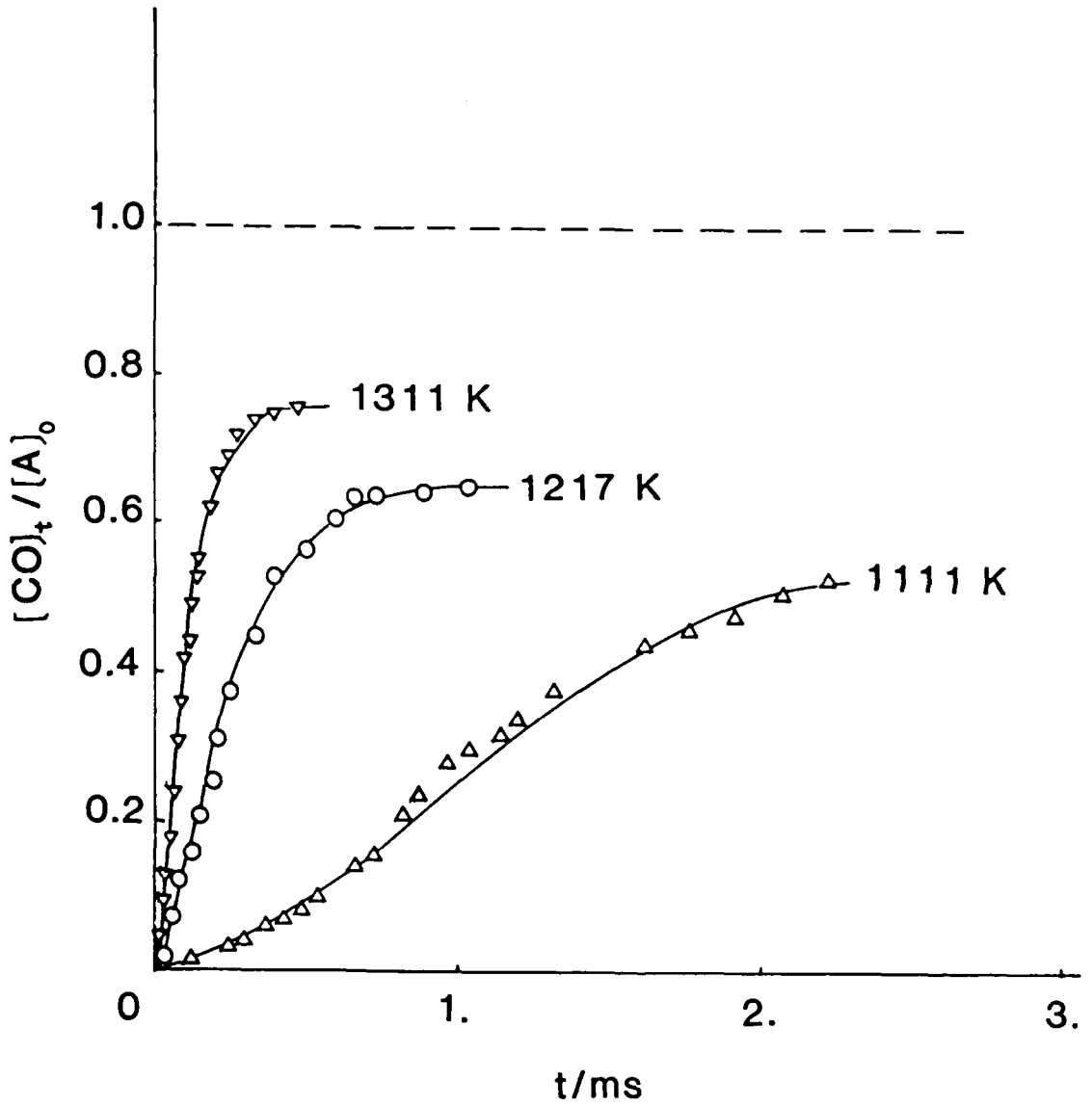

Fig. 2.

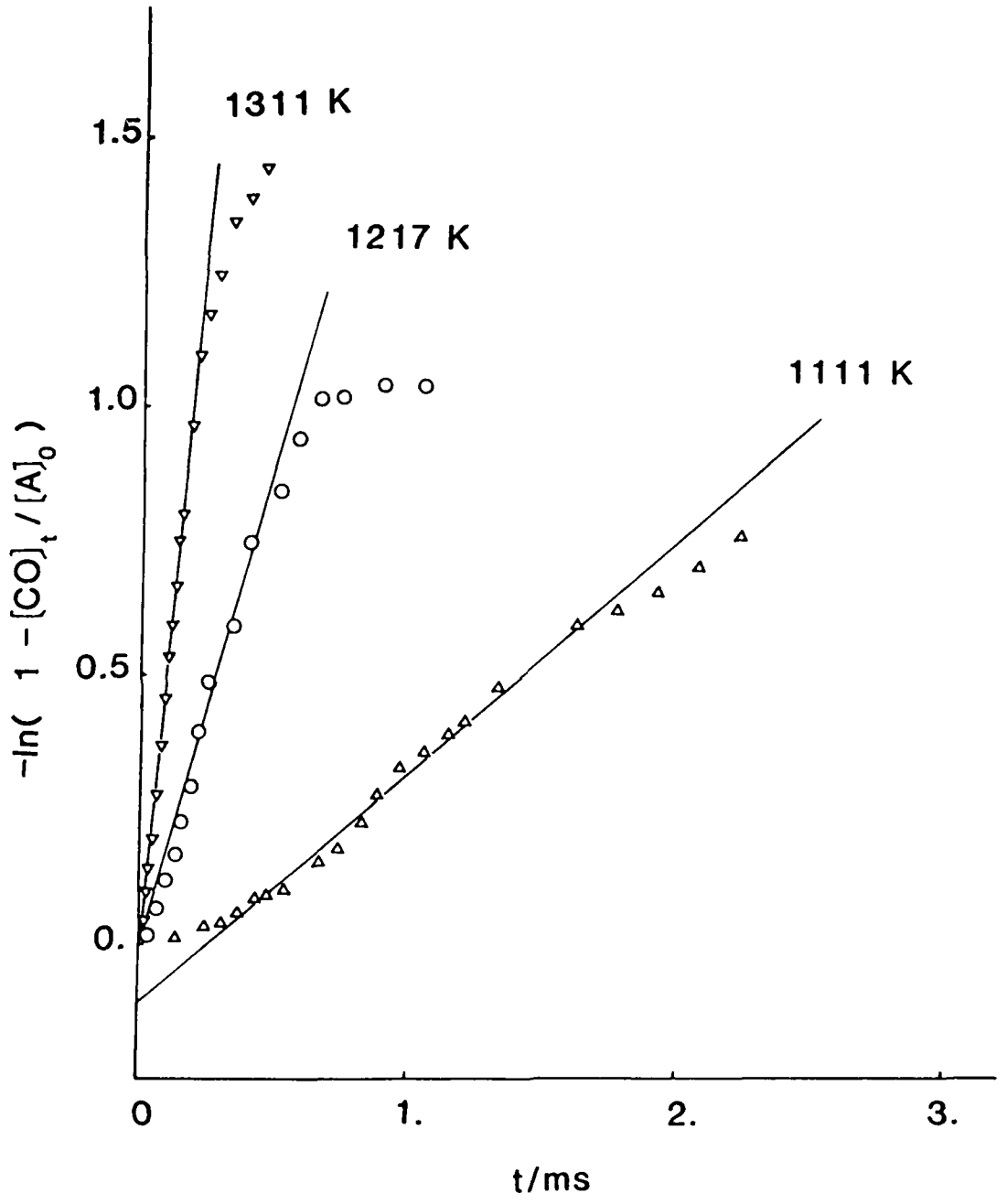

Fig. 3.

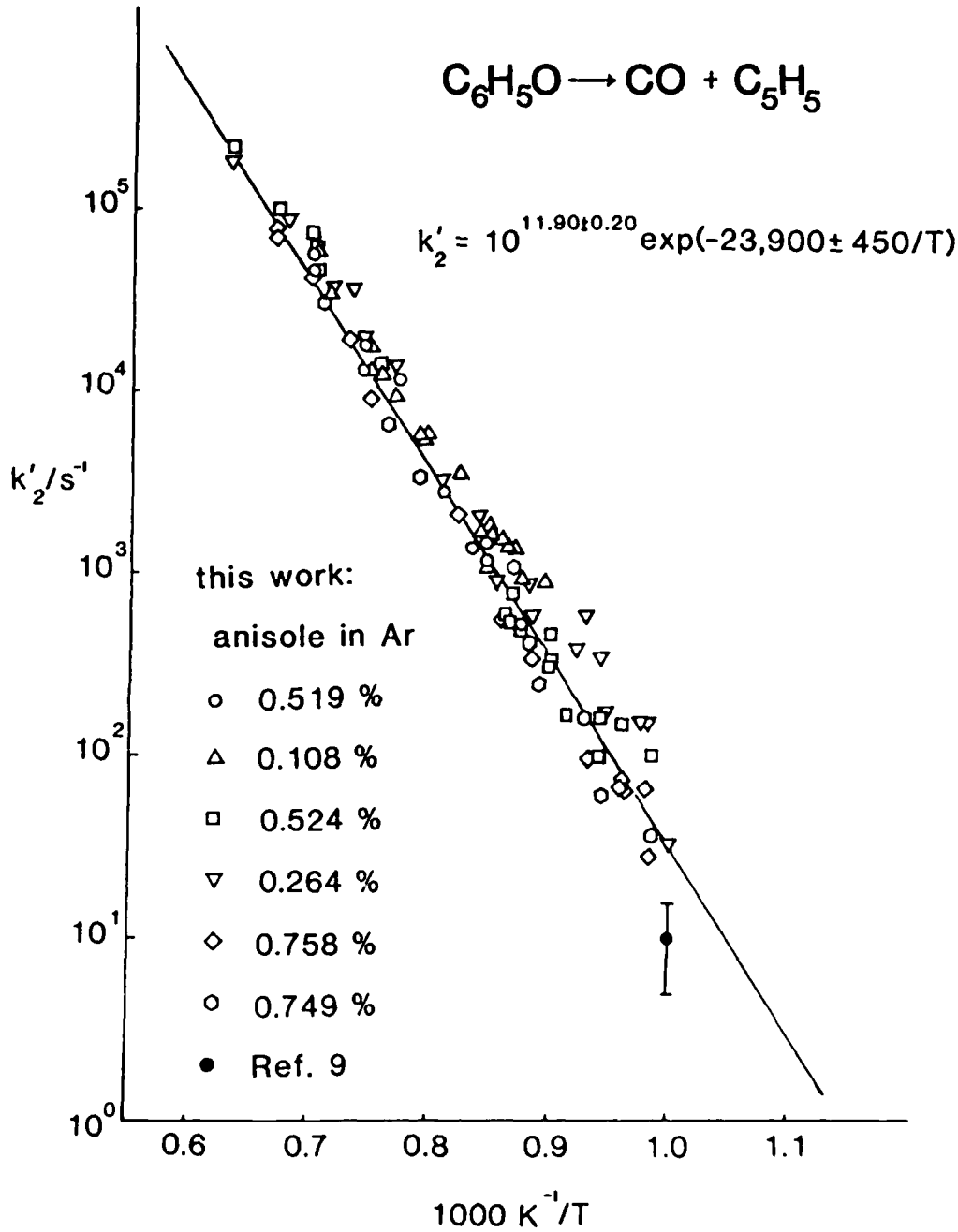
$C_6H_5O \rightarrow CO + C_5H_5$
$k'_2 = 10^{11.90\pm0.20} \exp(-23{,}900 \pm 450/T)$
k'_2/s^{-1}
10^5
10^4
10^3
10^2
10^1
10^0
this work:
anisole in Ar
0.519 %
0.108 %
0.524 %
0.264 %
0.758 %
0.749 %
Ref. 9
0.6
0.7
0.8
0.9
1.0
1.1
$1000\ K^{-1}/T$

Fig. 4.

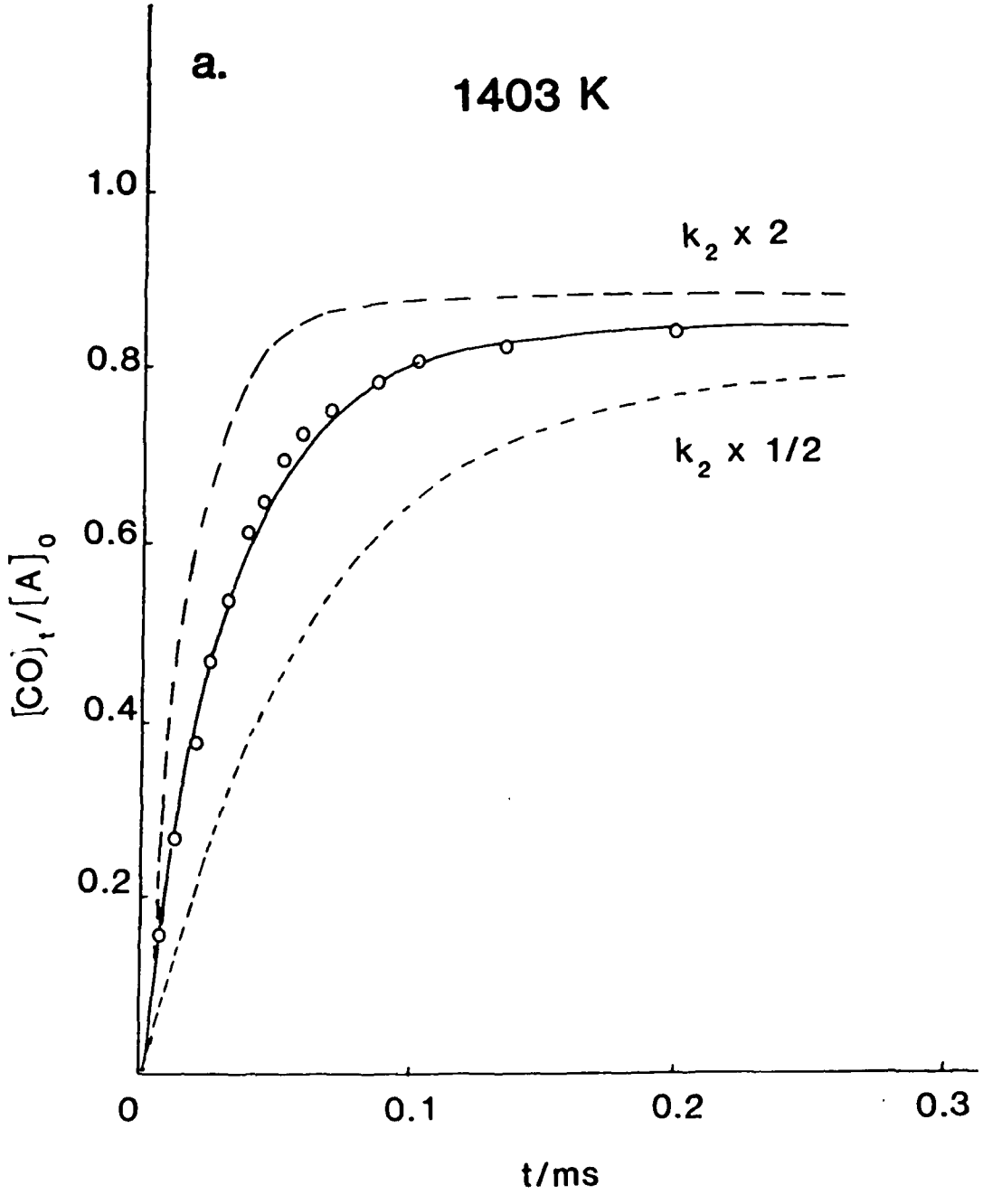

Fig. 5(a)

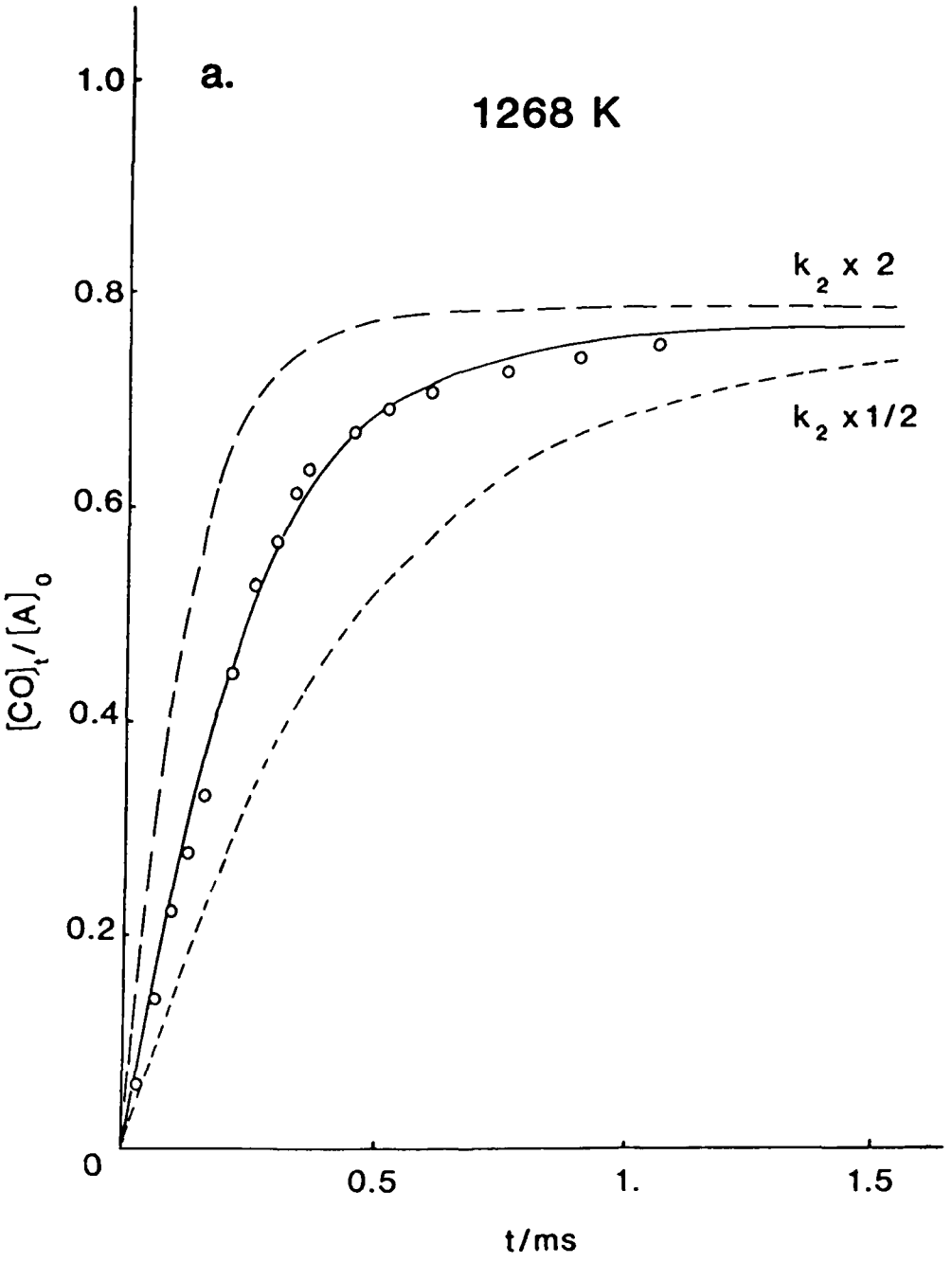

Fig. 6 (a)

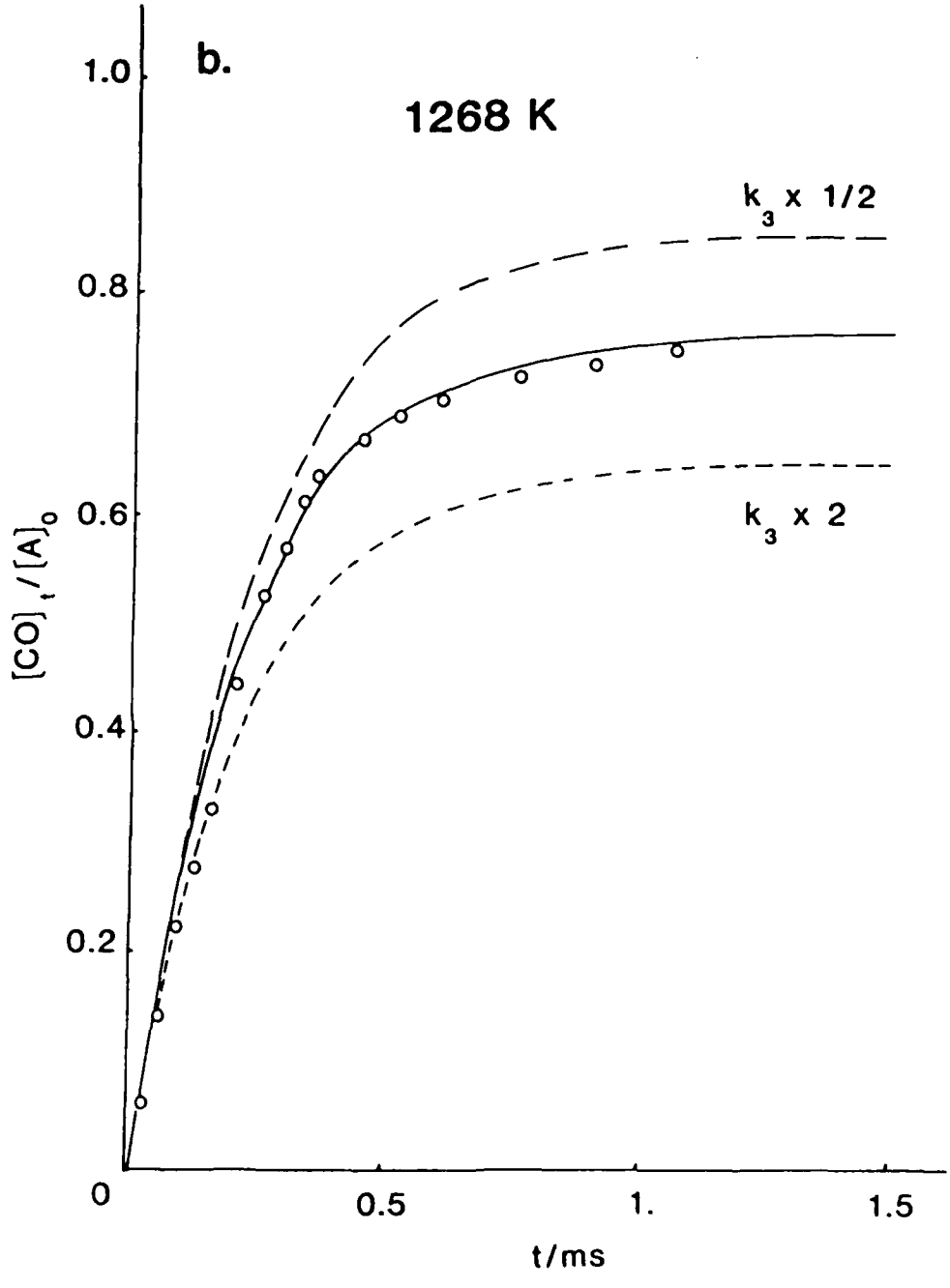

Fig. 6 (b).

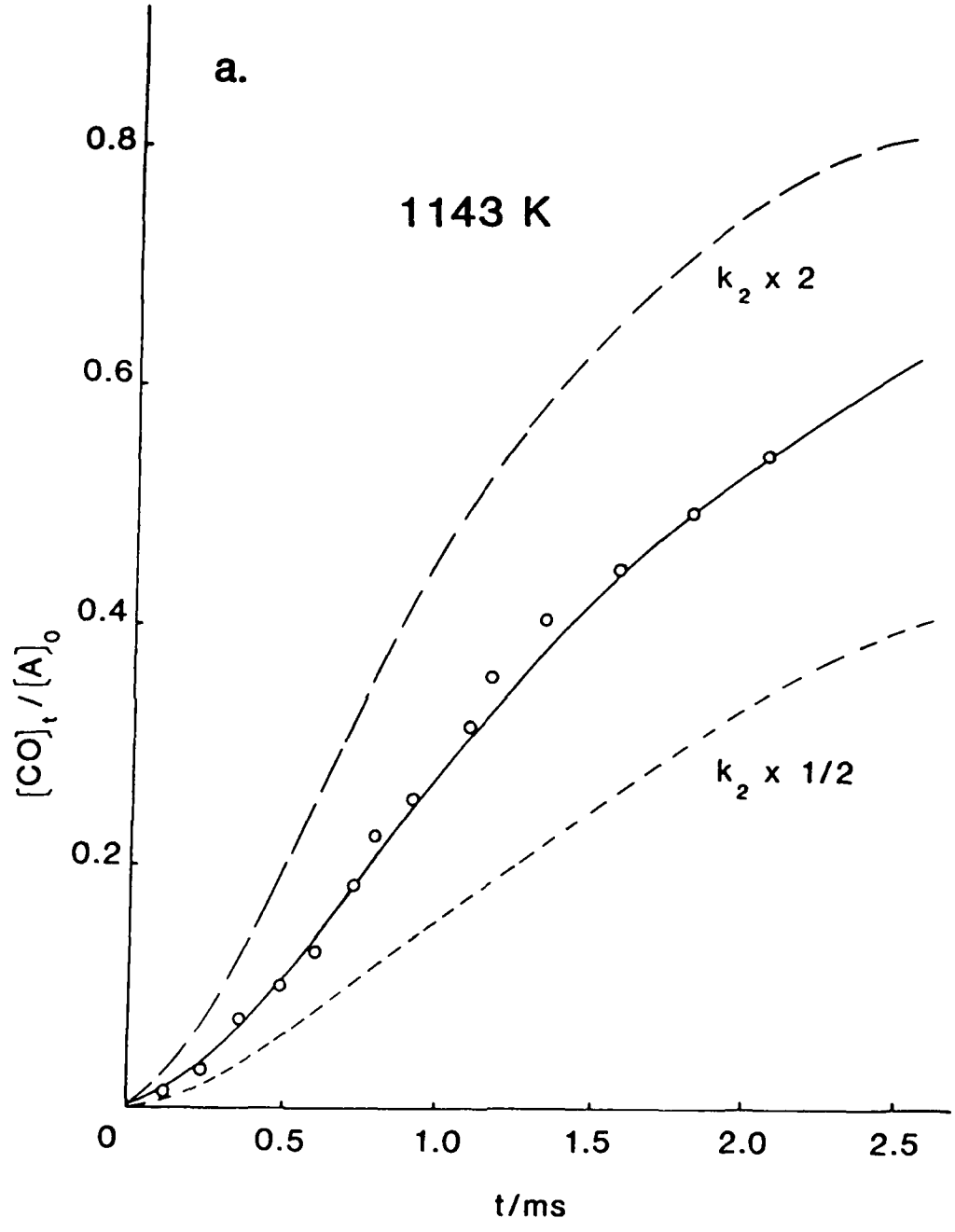

Fig. 7(a)

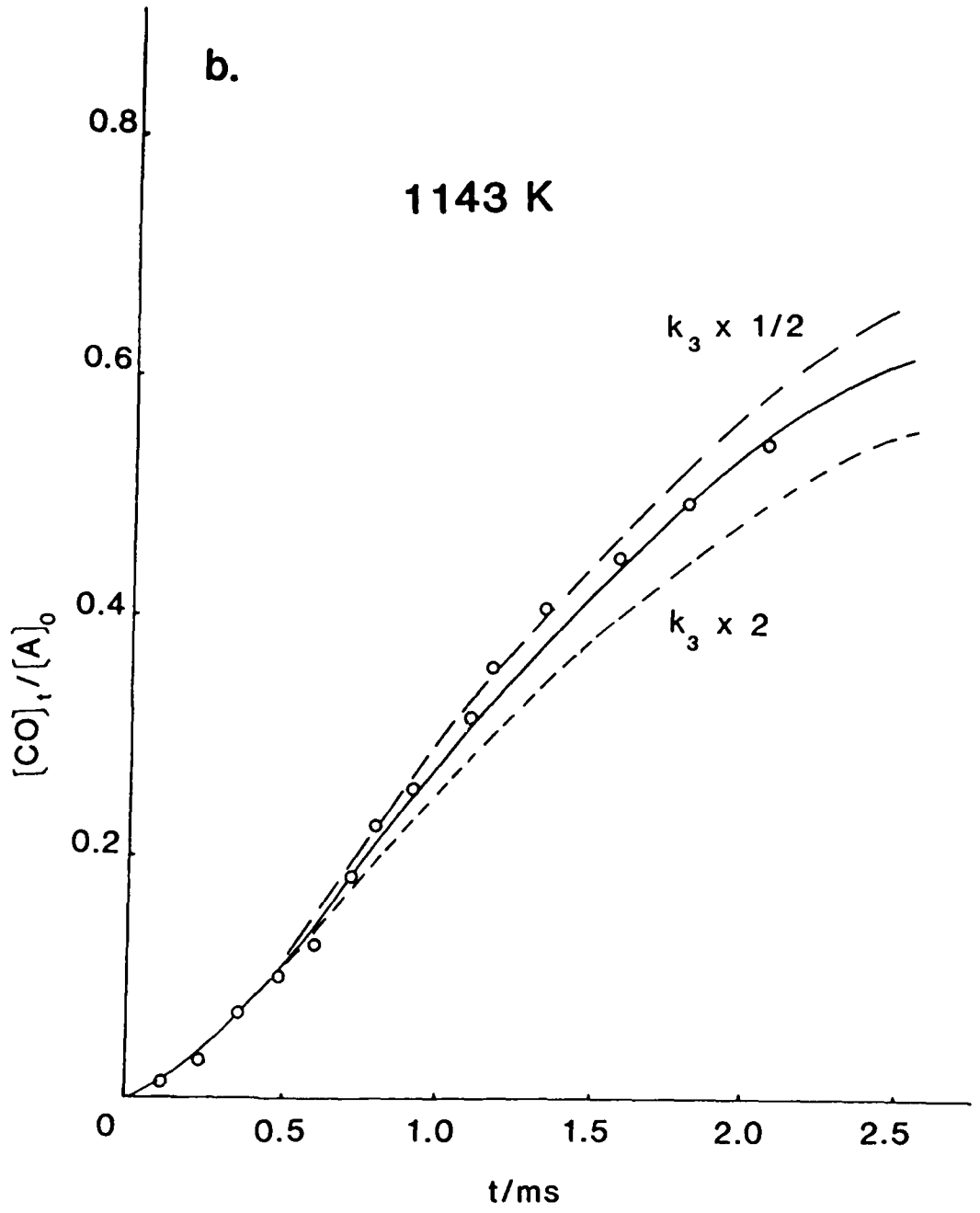

Fig. 7 (b)

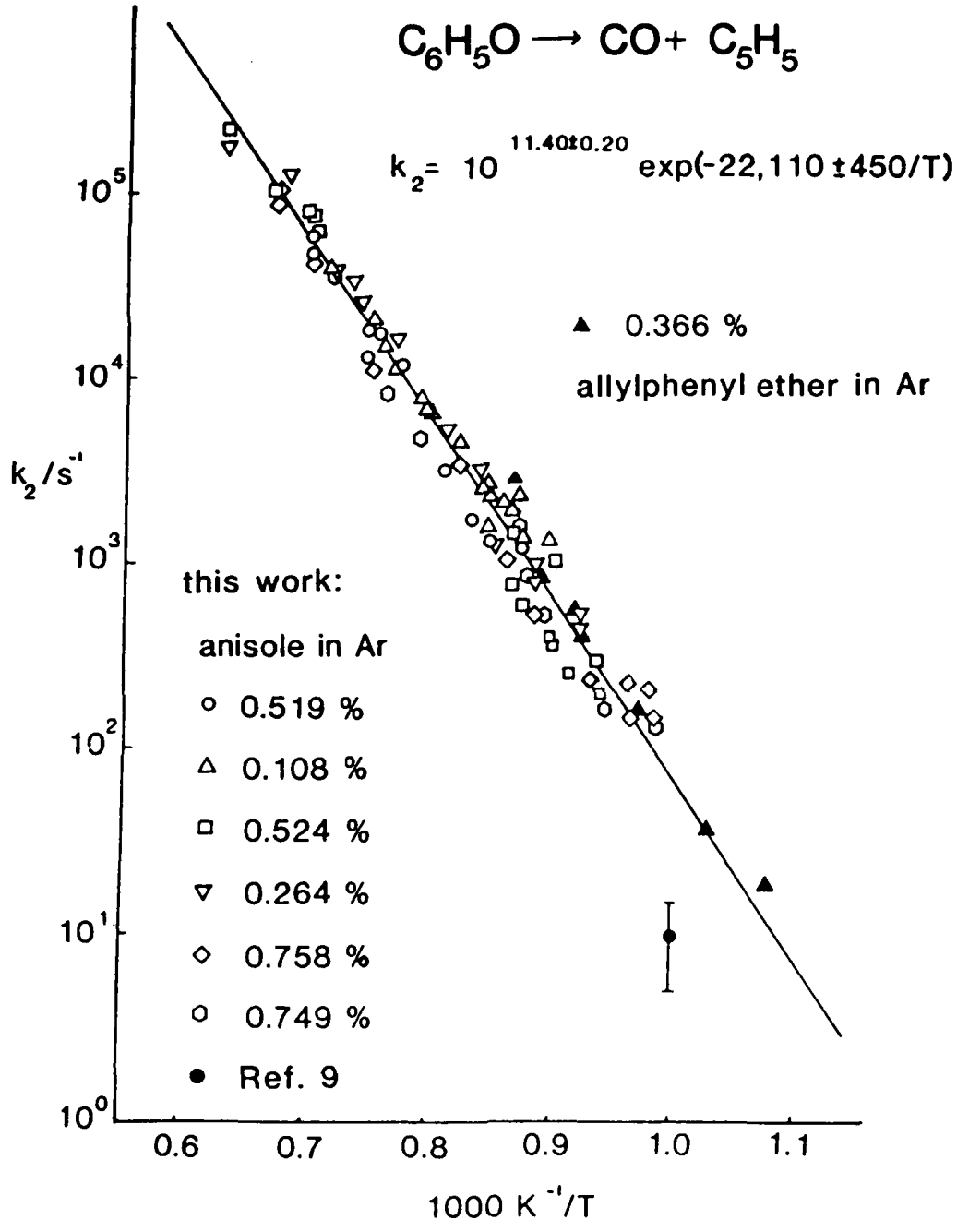
$C_6H_5O \rightarrow CO + C_5H_5$
$k_2 = 10^{11.40\pm0.20} \exp(-22,110 \pm 450/T)$
▲ 0.366 %
allylphenyl ether in Ar
this work:
anisole in Ar
○ 0.519 %
△ 0.108 %
□ 0.524 %
▽ 0.264 %
◇ 0.758 %
⬡ 0.749 %
● Ref. 9
k_2/s^{-1}
10^5
10^4
10^3
10^2
10^1
10^0
0.6
0.7
0.8
0.9
1.0
1.1
1000 K^{-1}/T

Fig. 8.

END

DTIC

4-86